



A Boosted Critical Temperature of 166 K in Superconducting D₃S Synthesized from Elemental Sulfur and Hydrogen

Vasily S. Minkov,* Vitali B. Prakapenka, Eran Greenberg, and Mikhail I. Erements

Abstract: The discovery of superconductivity in H₃S at 203 K marked an advance towards room-temperature superconductivity and demonstrated the potential of H-dominated compounds to possess a high critical temperature (*T_c*). There have been numerous reports of the H-S system over the last five years, but important questions remain unanswered. It is crucial to verify whether the *T_c* was determined correctly for samples prepared from compressed H₂S, since they are inevitably contaminated with H-depleted byproducts. Here, we prepare stoichiometric H₃S by direct in situ synthesis from elemental S and excess H₂. The Im $\bar{3}m$ phase of D₃S samples exhibits a *T_c* significantly higher than previously reported values (ca. 150 K), reaching a maximum *T_c* of 166 K at 157 GPa. Furthermore, we confirm that the sharp decrease in *T_c* below 150 GPa is accompanied by continuous rhombohedral structural distortions and demonstrate that the Cccm phase is non-metallic, with molecular H₂ units in the crystal structure.

Room-temperature superconductivity has been a long-standing endeavor in the fields of physics and material science. According to the Bardeen–Cooper–Schrieffer theory of superconductivity,^[1] high phonon frequencies and strong electron–phonon interactions are favorable for a high *T_c*, and hydrogen naturally appears as the best candidate.^[2] Although the formation of a metallic phase was recently reported,^[3] experimental evidence of superconductivity in hydrogen remains a major challenge, since it requires pressures of about 500 GPa.^[4] To decrease the pressure of metallization in pure hydrogen to accessible values, Ashcroft has suggested chemical precompression with heavier atoms.^[5]

While Group 4 hydrides, which were originally proposed for doped hydrogen, did not succeed, superconductivity was

observed near 200 K in compressed H₂S at about 150 GPa;^[6] these correlate with independent predictions for H₃S compositions with the same high *T_c*.^[7] Correlation between the observed superconductivity and proposed Im $\bar{3}m$ crystal lattice for H₃S was found experimentally shortly thereafter.^[8] There have been several theoretical and experimental studies of the H-S system.^[9] However, several questions remain unanswered. In particular, it is important to confirm whether *T_c* values were determined reliably for their particular superconducting phases, and to elucidate which phase of H₃S stoichiometry is responsible for the sharp decrease in *T_c* below 150 GPa.

Because Drozdov et al.^[6b] used H₂S as a starting compound, guided by predicted superconductivity in H₂S at 70 K,^[10] questions regarding the purity of samples arose from the very beginning. Indeed, Im $\bar{3}m$ H₃S can be prepared by disproportionation of H₂S.^[6b,8,11] However, such samples are likely contaminated by a H-depleted phase. Although predictions suggest that the only thermodynamically stable byproduct of the reaction is pure S above 113 GPa,^[12] experimental X-ray diffraction data indicate a complex composition: S content varies in different samples and is always smaller than expected, even at higher pressures of 140–190 GPa.^[8,11–13] The persistence of H₂S and H₄S₃ in samples at pressures above 140 GPa indicates that large kinetic barriers suppress decomposition.^[12]

The highest measured *T_c* for such samples is 203 K at 155 GPa in H₃S and 152 K at 173 GPa in D₃S.^[6b,9a,13a] *T_c* values for different samples^[6b,8,9a] are highly disperse (ca. 15 K), indicating poor crystallinity, inhomogeneity, and impurities in the superconducting phase. These imperfections can lower *T_c* compared to those observed with the ideal Im $\bar{3}m$ phase.

Guigou et al.^[14] and Goncharov et al.^[15] demonstrated that H₃S compounds of better crystallinity could be prepared via direct chemical synthesis from S and H₂. This approach yielded products without H-depleted impurities, since H₂ was used in excess. Electrical measurements for the directly synthesized Im $\bar{3}m$ phase of H₃S revealed *T_c* values of about 200 K at about 150 GPa.^[16] However, neither the pressure-dependence of *T_c*, nor data for the deuterium counterpart were reported.

Herein, we report a systematic study of compounds with H₃S and D₃S stoichiometry synthesized directly from laser-heated mixtures of S and excess H₂ (D₂). We present an enhanced *T_c* of 166 K for the Im $\bar{3}m$ phase of D₃S, evaluate the phase diagram of H₃S (D₃S) over the wide pressure range of 110–170 GPa, and discuss the electrical properties of the Cccm, R3m, and Im $\bar{3}m$ phases.

At high pressures, S reacts readily with H₂ giving final products with H₃S stoichiometry. The formation of particular

[*] V. S. Minkov, M. I. Erements
Max-Planck Institut für Chemie
Hahn-Meitner Weg 1, 55128 Mainz (Germany)
E-mail: v.minkov@mpic.de

V. B. Prakapenka
Center for Advanced Radiation Sources, University of Chicago
5640 South Ellis Avenue, 60637 Chicago, IL (USA)

E. Greenberg
Applied Physics Department, Soreq Nuclear Research Center
81800 Yavne (Israel)

Supporting information and the ORCID identification number(s) for the author(s) of this article can be found under:
<https://doi.org/10.1002/anie.202007091>.

© 2020 The Authors. Published by Wiley-VCH GmbH. This is an open access article under the terms of the Creative Commons Attribution Non-Commercial License, which permits use, distribution and reproduction in any medium, provided the original work is properly cited, and is not used for commercial purposes.

phases depends on the pressure at which the sulfur–hydrogen mixture is heated. At 111–132 GPa, the mixture yields the *Cccm* phase (samples 1–3) even with subtle laser-heating at 700–1000 K, whereas the *Im* $\bar{3}m$ phase requires pressures over 150 GPa and temperatures of 1500–2000 K (samples 4–6). In total, three H₃S and three D₃S samples were synthesized. The conditions for each in situ synthesis and the pressure ranges at which samples were studied are summarized in Figure 1 and Experimental Section (Supporting Information).

The *Cccm* phase is sustainable with further compression. Increasing the pressure to 152 GPa with subsequent laser heating does not initiate the phase transition to the more energetically favorable *Im* $\bar{3}m$ or *R3m* phases. The presence of the *Cccm* phase at significantly higher pressures than the predicted upper limit of about 100 GPa^[7] has also been observed earlier^[14,15] and indicates an extended metastable region for this phase.

The crystal structure and properties of the *Im* $\bar{3}m$ and *Cccm* phases differ dramatically (Figure 2). The *Im* $\bar{3}m$ phase is a metal with a strong metallic luster and a small resistance of < 0.5 Ω at room temperature, whereas the *Cccm* phase is an insulator with an electrical resistance of about 10⁶ Ω that does not decrease with cooling or compression. Refined crystal structures from XRD data for sample 1 and sample 4 agree with the theoretical *Cccm* and *Im* $\bar{3}m$ structural models, respectively.^[7]

In contrast to the Raman-inactive metallic *Im* $\bar{3}m$ phase of H₃S (D₃S), the *Cccm* phase has very strong Raman-active modes. Spectroscopic data can be used to extract valuable information about the H-sublattice, which cannot be derived from XRD data. Isotopic substitution within the *Cccm* phase

results in a redshift of about $\sqrt{2}$ for those Raman modes associated with vibrations involving H atoms. A broad Raman band for sulfhydryl groups at 2500 cm⁻¹ in H₃S and at 1860 cm⁻¹ in D₃S indicates the presence of strong S–H \cdots S H-bonds in the crystals.^[17] Two bands, at 3720 and 3875 cm⁻¹ in H₃S, and at 2735 and 2840 cm⁻¹ in D₃S, are assigned to H–H_{str} and D–D_{str} from the coordinated H₂ and D₂ molecular units in the *Cccm* phase, respectively (Figure 2c).

Compared to the Raman bands at 4010 cm⁻¹ for H–H_{str} and 3010 cm⁻¹ for D–D_{str}, observed for bulk H₂ (D₂) media around the H₃S (D₃S) samples, the redshift in the *Cccm* phase indicates a strengthened interaction between the H₂ (D₂) molecules and the rigid crystal framework. These data confirm the theoretical structural model for the *Cccm* phase of H₃S,^[7] which contains two crystallographically nonequivalent H₂ molecular units (Figure 2d). According to the model, the first type of H₂ in the lattice has a shorter H–H bond length and longer contacts to the closest S atoms, whereas the second type has a longer H–H bond and a shorter distance to the surrounding atoms. These predictions agree with the spectroscopic data: stronger coordination of molecular units of the second type causes increased elongation of the H–H bond and, therefore, a larger redshift for the H–H_{str} band in the Raman spectra.

Samples with the *Im* $\bar{3}m$ phase of H₃S (D₃S) demonstrate high *T*_c values at pressures ranging 150–170 GPa (Figure 3). Sample 4, for instance, has a *T*_c of 196 K at 148 GPa (Figure 3b). Owing to better sample crystallinity, the superconductive transitions are sharper and narrower than those reported for samples prepared from compressed H₂S (D₂S).^[6b,8] Recently published data for the *Im* $\bar{3}m$ phase of H₃S synthesized from S and H₂ also demonstrate similar *T*_c values of about 200 K at about 150 GPa.^[16] In summary, among numerous samples prepared from compressed H₂S,^[6] the highest observed *T*_c values compare well to values measured for samples synthesized from the elements.

In contrast to H₃S, the deuterium analogue demonstrates a significantly enhanced *T*_c, reaching a record 166 K at 157 GPa in sample 5 and 164 K at 161 GPa in sample 6. These values agree well with the predicted *T*_c of 159 K obtained from assumptions that the isotope effect is independent of pressure.^[18] Thus, the *T*_c for cubic D₃S synthesized from S and D₂ significantly exceeds, by about 15 K (or ca. 10%), the maximum value of 152 K measured previously for samples prepared via pressure-induced disproportionation of D₂S.^[6,8] The lower *T*_c values in such samples were likely caused by inferior crystallinity, inhomogeneity of the *Im* $\bar{3}m$ phase, contamination by D-depleted byproducts, and impurity of the initial D₂S source (97%).^[6b]

Further compression of the *Im* $\bar{3}m$ phase leads to a decrease in *T*_c to 194 K at 155 GPa for H₃S (sample 4) and to 163 K

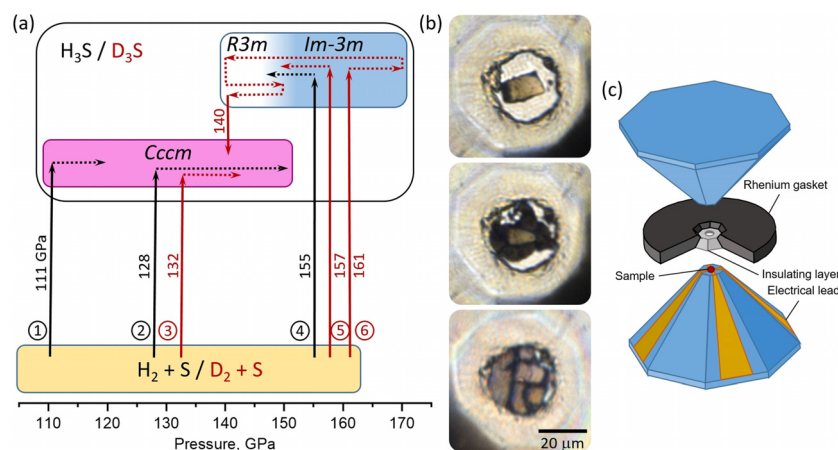


Figure 1. Synthesis of H₃S and D₃S from elemental S and H₂ (D₂). a) The conditions for laser-heating induced synthesis and the pressure ranges at which samples 1–6 were studied. Vertical arrows show the pressures at which the pulse laser was applied: heating initiates either the chemical reaction between S and H₂ (D₂) or the *R3m*-to-*Cccm* phase transition in D₃S. Black and red arrows correspond to the H-S and D-S systems, respectively. Horizontal dotted arrows show the pressure range over which the synthesized samples were studied. Colored boxes define the pressure ranges for the different phases. b) Photograph of sample 3 in the diamond anvil cell (DAC). At the top, a rectangular piece of S surrounded by D₂ is clamped in the round cavity in the insulating transparent gasket at 132 GPa. Two lower photographs demonstrate the formation of the *Cccm* phase of D₃S resulting from a chemical reaction after two successive laser treatments to about 700–800 K. c) Illustration of the diamond anvil assembly for the four-probe electrical measurements at high pressures.

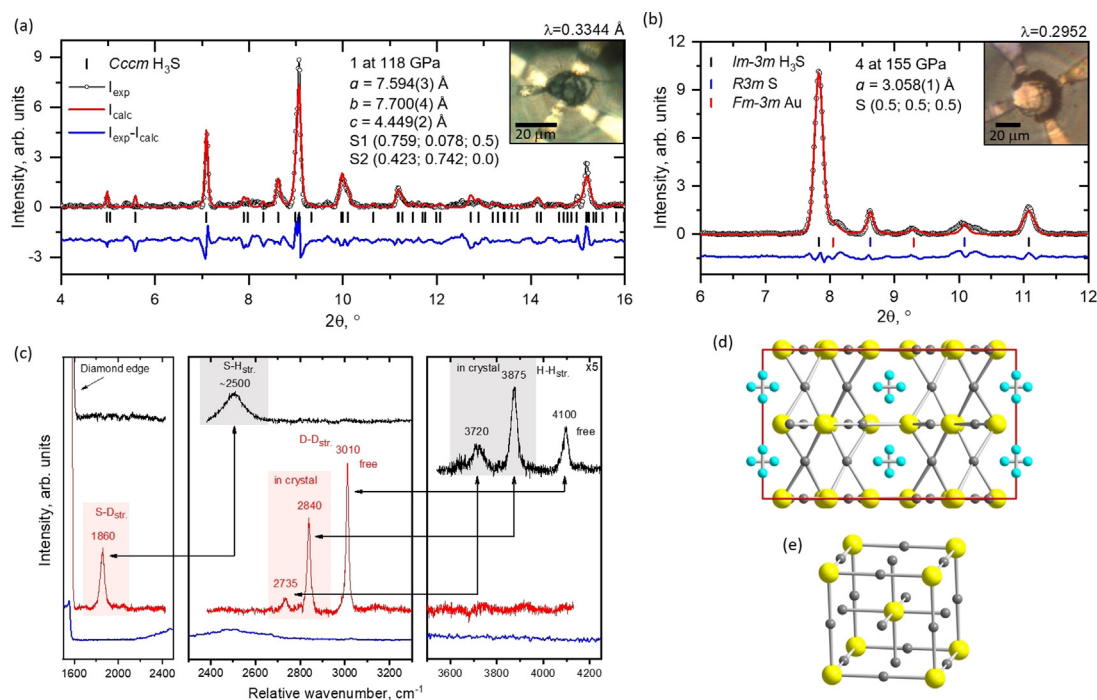


Figure 2. Structural data for H_3S samples synthesized from S and H_2 . a) Rietveld refinement for the $Cccm$ phase of H_3S at 118 GPa (sample 1), and b) $Im\bar{3}m$ phase of H_3S at 155 GPa (sample 4). Minor peaks in (b) originating from the β -Po phase of sulfur and the gold leads marked as blue and red dashes, respectively. Photos of the corresponding samples are shown on the upper-right corner. c) Typical Raman spectra for the $Cccm$ phases of H_3S and D_3S at high pressures: the blue spectrum corresponds to pure sulfur after metallization (sample 5 at 115 GPa); black and red spectra correspond to the $Cccm$ phases of H_3S in the heated sample 2 at 128 GPa and D_3S in the heated sample 3 at 132 GPa, respectively. Black arrows show the redshift in the H–H and S–H stretching vibrations after isotopic substitution. d), e) Fragments of the refined crystal structures for the $Cccm$ and $Im\bar{3}m$ phases of H_3S (H atoms were put in calculated positions^[7] and not refined). S and H atoms are shown as yellow and gray spheres, respectively; molecular H_2 units in the orthorhombic lattice are blue.

at 170 GPa for D_3S (sample 6). This behavior agrees with data for samples prepared from H_2S (D_2S)^[6b] and is provoked by pressure-induced hardening of the phonon frequencies.^[19]

Using the newly obtained data for T_c values in H_3S at 155 GPa and D_3S at 157 GPa, we calculated the isotope effect coefficient, $\alpha = -(\ln T_c^{D3S} - \ln T_c^{H3S}) / (\ln M^D - \ln M^H)$, where M^D and M^H are the atomic masses of D and H, respectively. The refined α for the $Im\bar{3}m$ phase is ≈ 0.22 , substantially smaller than both the value of about 0.42 derived from T_c values for disproportionated H_2S (D_2S)^[6b] and the expected canonical BCS value of 0.5. The low value of α likely stems from anharmonic effects.

Indeed, according to isotropic Migdal–Eliashberg equations, the calculated T_c for the $Im\bar{3}m$ phase of H_3S is 250 K; T_c decreases significantly to 194 K if anharmonic effects are considered.^[20] The computed T_c for the anharmonic case agrees well with the measured values. However, the same calculations for D_3S contradict the experiment and give 183 K and 152 K for harmonic and anharmonic approximations, respectively.^[20]

Next, we discuss dramatic changes in superconducting properties accompanying the $Im\bar{3}m$ -to- $R3m$ phase transformation. Decreasing pressure causes an abrupt drop in T_c to 93 K at 140 GPa for D_3S . Similar behavior is observed for samples prepared from compressed D_2S .^[6b,9a,19c] This trend is reversible and T_c is restored if pressure increases again (Figure 3). The decrease in T_c for D_3S is accompanied by structural changes. On decompression, the $Im\bar{3}m$ phase

becomes unstable and is distorted, decreasing the lattice symmetry to $R3m$. These rhombohedral distortions are more pronounced than previously predicted:^[7] further to a subtle reorientation of the H-sublattice and desymmetrization of the S–H–S bonds, the heavier S-sublattice also loses cubic symmetry. Changes in the S-sublattice manifest as splitting of the cubic phase reflections in X-ray powder patterns (Figure 4). This phase transition was not detected for samples prepared from H_2S (D_2S), likely because of broad reflections stemming from poorly crystallized H_3S (D_3S) compounds,^[8,11] but splitting was reported in the 110 and 211 reflections of the cubic phase for samples synthesized from S and H_2 (with improved crystals).^[15] The drastic rearrangement of the crystal structure also manifests in the Raman spectrum for the $R3m$ phase of D_3S , with two strong and narrow bands at 350 and 370 cm^{-1} and a composite broad band at 900–1100 cm^{-1} (Figure 4d). The metallic properties change as well; the sample loses metallic luster and its resistance increases. Annealing at about 1500 K and 140 GPa converts the structure from the $R3m$ into the $Cccm$ phase (Figure 4c).

These data clarify the phase diagram for H_3S (D_3S) and provide strong evidence that the $R3m$ phase is an intermediate metastable phase. The $R3m$ phase appears only on decompression, when the cubic phase is already unstable, but the phase transition to the thermodynamically more stable $Cccm$ phase is hindered by kinetic barriers. Taking structural features into account, the activation energy for the $Cccm$ -to- $Im\bar{3}m$ phase transition should contain not only the

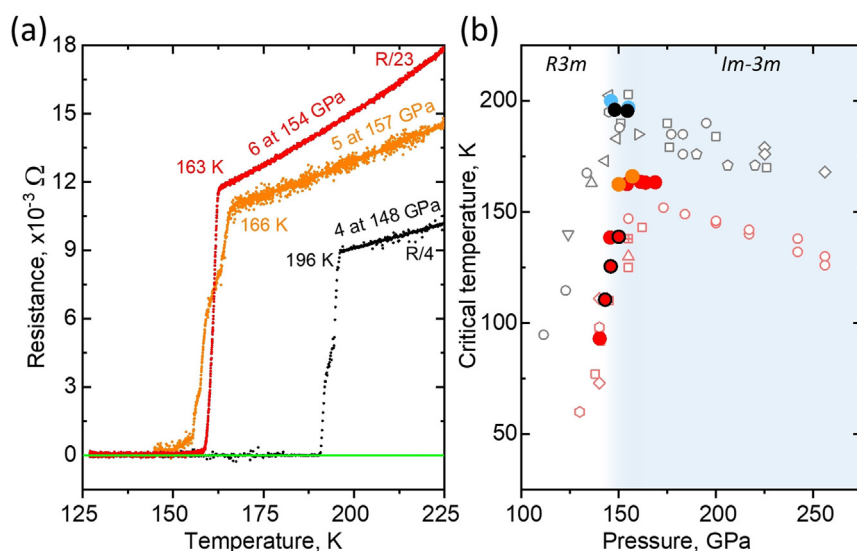


Figure 3. Four-probe electrical measurements for the superconducting phases of the synthesized H_3S and D_3S samples at high pressures. a) Temperature-dependence of electrical resistance for the $\text{Im}\bar{3}m$ phases of H_3S (sample 4, black) and D_3S (sample 5, orange; and sample 6, red) near 155 GPa. The absolute resistance values for samples 4 and 6 were divided by 4 and 23, correspondingly, for presentation. The green horizontal line is a guide for zero resistance. b) Summarized temperature dependence for the T_c observed in electrical measurements for different superconducting H_3S (black symbols) and D_3S (red symbols) samples reported to date. Data collected for H_3S and D_3S samples prepared from compressed H_2S and D_2S are shown as open symbols.^[6b, 8, 9a] Data for H_3S samples synthesized earlier from S and H_2 are shown as blue circles.^[16] Data measured in the present study are shown as black, red, and orange circles (consistent with coloring for samples 4, 5, and 6 in Figure 3 a). Red circles with black frames correspond to sample 6 on subsequent compression from 140 to 150 GPa. The white and blue regions define the pressure ranges where the $R3m$ and $\text{Im}\bar{3}m$ phases of H_3S and D_3S are stable.

energy required for the crystal lattice rearrangement, but also the energy needed to dissociate H_2 molecular units in the crystal. In fact, experimental data support the high activation energy value. The $Cccm$ phase survives increasing pressures up to at least 160 GPa,^[14] and the distorted cubic phase ($R3m$) persists on decompression at least down to 70 GPa, at which point only heating the sample to 1300 K triggers the transition to the $Cccm$ phase.^[15]

This new insight into the phase diagram for H_3S (D_3S) explains why Drozdov et al. were able to produce samples with high T_c values from H_2S via low-temperature compression and annealing above 150 GPa. The superconducting phases of the H_3S composition could not be synthesized by annealing pressurized samples with H_2S below 150 GPa, since the only thermodynamically stable phase of H_3S at these pressures is $Cccm$. Neither could they be prepared by continuous compression of H_2S at room temperature, because the measured T_c values for such samples never exceed 80 K (or 40 K for the D-S system), even at higher pressures up to 190 GPa.^[6] Low-temperature pressurizing prevented chemical decomposition and disproportionation of H_2S , allowing it to exist at pressures at which the $\text{Im}\bar{3}m$ phase of H_3S is thermodynamically stable.

In summary, we synthesized stoichiometric H_3S and D_3S from elemental S and excess H_2 (D_2) at 111–161 GPa and refined the phase diagram for the $Cccm$, $\text{Im}\bar{3}m$, and $R3m$ phases of H_3S (D_3S). We revealed that the synthesized $\text{Im}\bar{3}m$

D_3S samples exhibit reproducible increased T_c values of up to 166 K at 157 GPa and confirmed that continuous distortions of the cubic phase into the $R3m$ phase cause a sharp decrease in T_c below 150 GPa. Moreover, we demonstrated that the $Cccm$ phase is non-metallic, with molecular H_2 (D_2) units in the crystal structure.

Acknowledgements

The synchrotron X-Ray diffraction data were collected at GeoSoilEnviro CARS (The University of Chicago, Sector 13), Advanced Photon Source (APS), Argonne National Laboratory (USA). GeoSoilEnviro CARS is supported by the National Science Foundation-Earth Sciences (EAR-1634415) and Department of Energy-GeoSciences (DE-FG02-94ER14466). This research used resources of the Advanced Photon Source, a U.S. Department of Energy (DOE) Office of Science User Facility operated for the DOE Office of Science by Argonne National Laboratory under Contract No. DE-AC02-06CH11357. We thank I. Errea for helpful discussions. Open access funding enabled and organized by Projekt DEAL.

Conflict of interest

The authors declare no conflict of interest.

Keywords: high-pressure chemistry · hydrogen sulfide · isotope effects · superconductors

- [1] J. Bardeen, L. N. Cooper, J. R. Schrieffer, *Phys. Rev.* **1957**, *108*, 1175–1204.
- [2] a) E. Wigner, H. B. Huntington, *J. Chem. Phys.* **1935**, *3*, 764–770; b) N. W. Ashcroft, *Phys. Rev. Lett.* **1968**, *21*, 1748–1749; c) V. L. Ginzburg, *J. Stat. Phys.* **1969**, *1*, 3–24.
- [3] a) R. P. Dias, I. F. Silvera, *Science* **2017**, *355*, 715–718; b) M. I. Eremets, A. P. Drozdov, P. P. Kong, H. Wang, *Nat. Phys.* **2019**, *15*, 1246–1249; c) P. Loubeyre, F. Occelli, P. Dumas, *Nature* **2020**, *577*, 631–635.
- [4] C. J. Pickard, R. J. Needs, *Nat. Phys.* **2007**, *3*, 473–476.
- [5] N. W. Ashcroft, *Phys. Rev. Lett.* **2004**, *92*, 187002.
- [6] a) A. P. Drozdov, M. I. Eremets, I. A. Troyan, *arXiv* **2014**, arXiv:1412.0460; b) A. P. Drozdov, M. I. Eremets, I. A. Troyan, V. Ksenofontov, S. I. Shylin, *Nature* **2015**, *525*, 73–76.
- [7] D. Duan, Y. Liu, F. Tian, D. Li, X. Huang, Z. Zhao, H. Yu, B. Liu, W. Tian, T. Cui, *Sci. Rep.* **2014**, *4*, 6968.
- [8] M. Einaga, M. Sakata, T. Ishikawa, K. Shimizu, M. Eremets, A. Drozdov, I. Troyan, N. Hirao, Y. Ohishi, *Nat. Phys.* **2016**, *12*, 835–839.

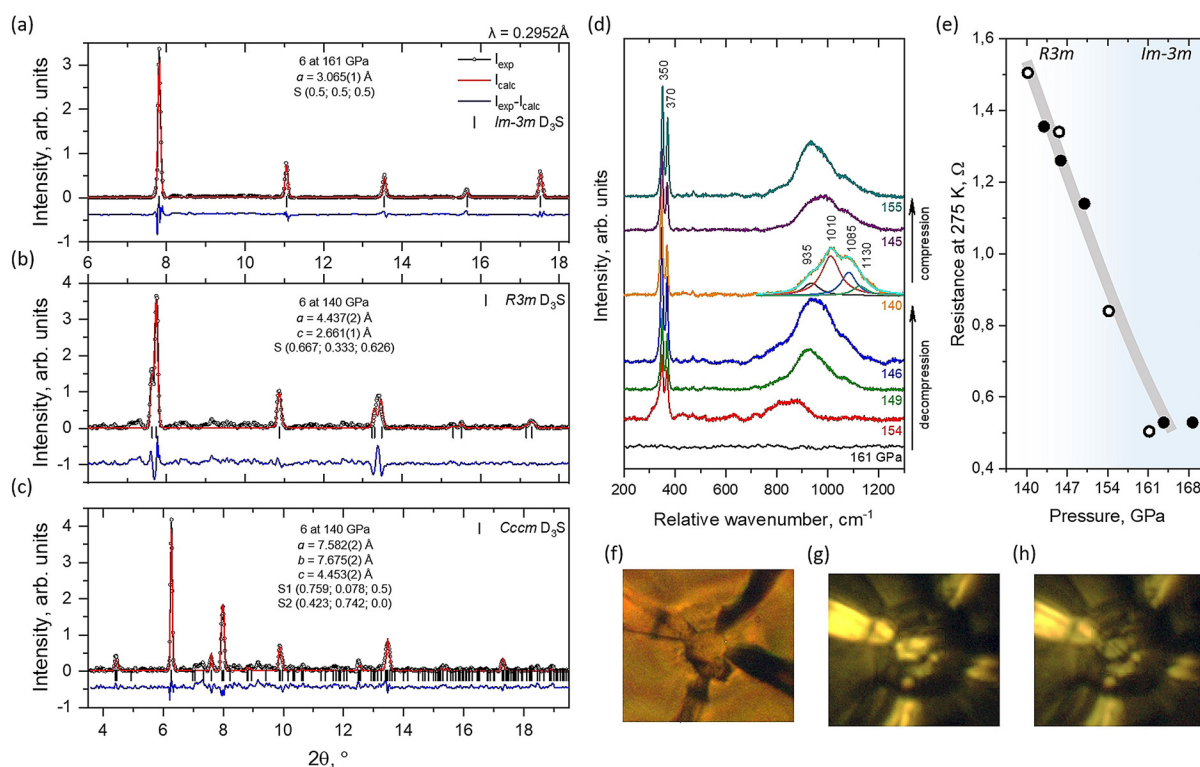


Figure 4. Transformation of the $Im\bar{3}m$ phase of D_3S to the $R3m$ and $Cccm$ phases on decompression of sample 6. a) Rietveld refinement for the $Im\bar{3}m$ phase after heating the S and D_2 mixture at 161 GPa, b) the $R3m$ phase after decreasing the pressure to 140 GPa, and c) the $Cccm$ phase after subsequent heating to about 1500 K at 140 GPa. d) Raman spectra of sample 6 on decompression. The orange spectrum corresponds to the $R3m$ phase of D_3S at 140 GPa, illustrated in (b). The broad band at 900–1200 cm^{-1} is fitted by four single modes. e) The reversible change in resistance for the $R3m$ and $Im\bar{3}m$ phases of D_3S at room temperature on decompression (open circles) and pressurizing (filled circles). f)–h) Photographs of sample 6 taken under reflected illumination at decreasing pressure: f) the $Im\bar{3}m$ phase at 161 GPa, g) the $R3m$ phase at 140 GPa, and h) the $Cccm$ phase of D_3S at 140 GPa. Metallic luster reduces after each phase transition.

- [9] a) M. I. Erements, A. P. Drozdov, *Phys.-Usp.* **2016**, *59*, 1154–1160; b) L. Zhang, Y. Wang, J. Lv, Y. Ma, *Nat. Rev. Mater.* **2017**, *2*, 17005; c) T. Bi, N. Zarifi, T. Terpstra, E. Zurek, *arXiv* **2018**, arXiv:1806.00163; d) L. P. Gor'kov, V. Z. Kresin, *Rev. Mod. Phys.* **2018**, *90*, 011001; e) L. Pietronero, L. Boeri, E. Cappelluti, L. Ortenzi, *Quantum Stud. Math. Found.* **2018**, *5*, 5–21; f) C. J. Pickard, I. Errea, M. I. Erements, *Annu. Rev. Condens. Matter Phys.* **2020**, *11*, 57–76; g) W. Pickett, M. Erements, *Phys. Today* **2019**, *72*, 52–58; h) J. A. Flores-Livas, L. Boeri, A. Sanna, G. Profeta, R. Arita, M. I. Erements, *Phys. Rep.* **2020**, *856*, 1–78; i) K. Shimizu, *J. Phys. Soc. Jpn.* **2020**, *89*, 051005.
- [10] Y. Li, J. Hao, H. Liu, Y. Li, Y. Ma, *J. Chem. Phys.* **2014**, *140*, 174712.
- [11] A. F. Goncharov, S. S. Lobanov, I. Kruglov, X. M. Zhao, X. J. Chen, A. R. Oganov, Z. Konôpková, V. B. Prakapenka, *Phys. Rev. B* **2016**, *93*, 174105.
- [12] Y. Li, L. Wang, H. Liu, Y. Zhang, J. Hao, C. J. Pickard, J. R. Nelson, R. J. Needs, W. Li, Y. Huang, I. Errea, M. Calandra, F. Mauri, Y. Ma, *Phys. Rev. B* **2016**, *93*, 020103.
- [13] a) K. Shimizu, M. Einaga, M. Sakata, A. Masuda, H. Nakao, M. Erements, A. Drozdov, I. Troyan, N. Hirao, S. Kawaguchi, Y. Ohishi, *Physica C* **2018**, *552*, 27–29; b) M. Einaga, M. Sakata, A. Masuda, H. Nakao, K. Shimizu, A. Drozdov, M. Erements, S. Kawaguchi, N. Hirao, Ohishi, *Jpn. J. Appl. Phys.* **2017**, *56*, 05FA13.
- [14] B. Guigue, A. Marizy, P. Loubeyre, *Phys. Rev. B* **2017**, *95*, 020104.
- [15] A. F. Goncharov, S. S. Lobanov, V. B. Prakapenka, E. Greenberg, *Phys. Rev. B* **2017**, *95*, 140101.
- [16] a) S. Mozaffari, D. Sun, V. S. Minkov, A. P. Drozdov, D. Knyazev, J. B. Betts, M. Einaga, K. Shimizu, M. I. Erements, L. Balicas, F. F. Balakirev, *Nat. Commun.* **2019**, *10*, 2522; b) H. Nakao, M. Einaga, M. Sakata, M. Kitagaki, K. Shimizu, S. Kawaguchi, N. Hirao, Y. Ohishi, *J. Phys. Soc. Jpn.* **2019**, *88*, 123701.
- [17] a) B. Krebs, G. Henkel, W. Stucker, *Z. Kristallogr.* **1984**, *39*, 43–49; b) G. R. Desiraju, T. Steiner, *Weak hydrogen bond in structural chemistry and biology*, Oxford, Oxford University Press, **1999**, p. 507.
- [18] A. P. Durajski, R. Szczesniak, L. Pietronero, *Ann. Phys.* **2016**, *528*, 358–364.
- [19] a) J. E. Hirsch, F. Marsiglio, *Physica C* **2015**, *511*, 45–49; b) R. Akashi, M. Kawamura, S. Tsuneyuki, Y. Nomura, R. Arita, *Phys. Rev. B* **2015**, *91*, 224513; c) X. Huang, X. Wang, D. Duan, B. Sundqvist, X. Li, Y. Huang, H. Yu, F. Li, Q. Zhou, B. Liu, T. Cui, *Nat. Sci. Rev.* **2019**, *6*, 713–718.
- [20] I. Errea, M. Calandra, C. J. Pickard, J. Nelson, R. J. Needs, Y. Li, H. Liu, Y. Zhang, Y. Ma, F. Mauri, *Phys. Rev. Lett.* **2015**, *114*, 157004.

Manuscript received: May 16, 2020

Accepted manuscript online: July 6, 2020

Version of record online: August 26, 2020